PLOS ONE

RESEARCH ARTICLE

Use of count-based image reconstruction to evaluate the variability and repeatability of measured standardised uptake values

Tomohiro Kaneta[1]*, Hiromitsu Daisaki[2], Matsuyoshi Ogawa[1], En-Tao Liu[1], Hitoshi Iizuka[1], Tetsu Arisawa[1], Ayako Hino-Shishikura[1], Keisuke Yoshida[1], Tomio Inoue[1]

1 Department of Radiology, Yokohama City University, Yokohama, Japan, **2** Department of Radiological Technology, Gunma Prefectual College of Health Sciences, Maebashi, Japan

* kaneta@yokohama-cu.ac.jp

Citation: Kaneta T, Daisaki H, Ogawa M, Liu E-T, Iizuka H, Arisawa T, et al. (2018) Use of count-based image reconstruction to evaluate the variability and repeatability of measured standardised uptake values. PLoS ONE 13(2): e0192549. https://doi.org/10.1371/journal.pone.0192549

Editor: Pradeep K. Garg, Biomedical Research Foundation, UNITED STATES

Received: October 11, 2017

Accepted: January 25, 2018

Published: February 12, 2018

Data Availability Statement: All relevant data are within the paper.

Funding: The authors received no specific funding for this work.

Competing interests: The authors have declared that no competing interests exist.

Abstract

Standardized uptake values (SUVs) are the most widely used quantitative imaging biomarkers in PET. It is important to evaluate the variability and repeatability of measured SUVs. Phantom studies seem to be essential for this purpose; however, repetitive phantom scanning is not recommended due to the decay of radioactivity. In this study, we performed count-based image reconstruction to avoid the influence of decay using two different PET/CT scanners. By adjusting the ratio of ^{18}F-fluorodeoxyglucose solution to tap water, a NEMA IEC body phantom was set for SUVs of 4.0 inside six hot spheres. The PET data were obtained using two scanners (*Aquiduo* and *Celesteion;* Toshiba Medical Systems, Tochigi, Japan). We set the start time for image reconstruction when the total radioactivity in the phantom was 2.53 kBq/cc, and employed the counts of the first 2-min acquisition as the standard. To maintain the number of counts for each image, we set the acquisition time for image reconstruction depending on the decay of radioactivity. We obtained 50 images, and calculated the SUV_{max} and SUV_{peak} of all six spheres in each image. The average values of the SUV_{max} were used to calculate the recovery coefficients to compare those measured by the two different scanners. Bland-Altman analyses of the SUVs measured by the two scanners were also performed. The measured SUVs using the two scanners exhibited a 10–30% difference, and the standard deviation (SD) of the measured SUVs was between 0.1–0.2. The *Celesteion* always exhibited higher values than the *Aquiduo*. The smaller sphere exhibited a larger SD, and the SUV_{peak} had a smaller SD than the SUV_{max}. The Bland-Altman analyses showed poor agreement between the SUVs measured by the two scanners. The recovery coefficient curves obtained from the two scanners were considerably different. The *Celesteion* exhibited higher recovery coefficients than the *Aquiduo*, especially at approximately 20-mm-diameter. Additionally, the curves were lower than those calculated from the standard 30-min acquisition images. We propound count-based image reconstruction to evaluate the variability and repeatability of measured SUVs. These results are also applicable for the standardization and harmonization of SUVs in multi-institutional studies.

Introduction

The standardized uptake value (SUV) is the most widely used quantitative imaging biomarker (QIB) in the field of positron emission tomography (PET). This quantitative value has been used to determine and evaluate differential diagnoses, therapeutic effects, and prognostic predictions [1–5]. It is well known that SUVs are influenced by many factors, such as the type of scanner and workstation, imaging protocol, body habitus, disease distribution, image noise, and radioactivity [6–8]. Recently, the Radiological Society of North America (RSNA) organized a Quantitative Imaging Biomarkers Alliance (QIBA) to improve the value and practicability of quantitative imaging biomarkers by reducing variability across devices, patients, and time [9]. To evaluate the variability and repeatability of measured SUVs, phantom studies seem to be essential. However, a standard method to evaluate them has yet to be established. One of the simplest methods may be repetitive scanning of a phantom. However, this method does not consider maintaining the condition of the phantom, even if repetitive scanning of the same phantom is performed continuously. The measured SUV will increase over time due to the increase of noise from the decay of radioactivity [10]. Thus, it is essential to design a method of repetitive phantom scanning that avoids the influence of radioactive decay. We therefore developed a method that maintains the total count for each image, by setting the time and duration for image reconstruction. In the current study, we performed this count-based image reconstruction (using a fixed average number of counts per image) instead of time-based image reconstruction (using a fixed acquisition time per image), and evaluated the variability and repeatability of measured SUVs using two different PET/computed tomography (CT) scanners.

Methods

Phantom preparation

An image-quality, International Electrotechnical Commission (IEC) body phantom of the type described in the National Electrical Manufacturers Association (NEMA) NU-2 2012 Standard [11] was used for the experiments. First, we measured the background volume of the phantoms. Then, using a regularly checked dose calibrator and taking decay into consideration, ^{18}F-fluorodeoxyglucose (FDG) solution was prepared and measured. Next, exactly one-fourth of the background volume was filled with tap water, and a precise amount of ^{18}F-FDG was added to produce a hot solution. An aliquot of this solution was added into all six (10-, 13-, 17-, 22-, 28-, and 37-mm-diameter) hot spheres. The phantom background was filled with tap water and stirred to produce a warm solution. The resultant SUV of each sphere was 4.0. The radioactivity of the ^{18}F-FDG used for the experiments was measured and corrected using a standard radiation source (^{68}Ge Dose Calibrator Source [37 MBq] BM06S-CE; RadQual Global Sources, NH, USA).

PET/CT scan

We used two different PET/CT scanners, developed by Toshiba Medical Systems (*Aquiduo* and *Celesteion*; Tochigi, Japan); both scanners combine a 16-multislice CT scanner with a high-resolution PET scanner. The *Aquiduo* scanner was released in 2005, and uses lutetium oxyorthosilicate (LSO) as detector material [12]. The *Celesteion* scanner was released in 2014, and uses lutetium-yttrium oxyorthosilicate (LYSO) with a time-of-flight (TOF) function. The TOF temporal resolution was reported to be < 450 ps by Toshiba [13].

A CT transmission scan was performed using a 120-kV tube voltage. The field-of-view (FOV) was set at 500 mm for the *Aquiduo* scanner, and 550 mm for the *Celesteion* scanner.

Subsequently, two consecutive 2-h PET emission scans were performed using list-mode (total, 4 h). Two hours is the maximum duration of continuous scanning for these scanners.

For reconstruction, a two-dimensional (2D) ordered subset expectation maximization (OSEM) algorithm was used for the *Aquiduo* scanner, and a three-dimensional (3D) OSEM algorithm was used for the *Celesteion*. The TOF function was used for the *Celesteion*. The pixel size was 2 mm for both scanners, and post-reconstruction Gaussian filtering was applied with a 6-mm full-width at half-maximum (FWHM) for the *Aquiduo* scanner, and a 7-mm FWHM for the *Celesteion*. These are the protocols used for daily clinical PET examinations in our hospital.

Count-based reconstruction

To maintain the number of counts for each image, we set the start time and duration for image reconstruction depending on the decay of radioactivity. In Japan, 3.7 kBq/kg of ^{18}F-FDG is commonly administered one hour prior to PET scan commencement. This corresponds to 2.53 kBq/cc at the beginning of the scan. We set the start time for image reconstruction when the total radioactivity in the phantom was 2.53 kBq/cc, and employed the counts of the first image reconstruction as the standard. Considering the measured radioactivity in the phantom and the decay of ^{18}F-FDG (109 min), the start time and duration for image reconstruction were determined to make the total counts in each reconstruction match (Table 1).

For example, for the first image reconstruction, the data were obtained between (A) and (A) + 02:00 (acquisition time: 2 min); the second reconstruction was obtained between (A) + 02:00 and (A) + 04:02 (2 min 2 sec), and the third between (A) + 04:02 and (A) + 06:05 (2 min 3 sec), where (A) was the time when the total radioactivity in the phantom corresponded to 2.53 kBq/cc. Fifty images were reconstructed for each scanner. For comparison, we also reconstructed images every 2 min.

SUV measurements

The SUV_{max} and SUV_{peak} of all six spheres in the 50 reconstructed images were calculated using GI-PET (AZE Co. Ltd., Tokyo, Japan). The SUV_{peak} was defined as the average SUV within a small sphere (12-mm-diameter) centred on the highest uptake region in the volume of interest (VOI), in contrast to the SUV_{max}, which was defined as the most intense voxel within the VOI. Both the SUV_{max} and SUV_{peak} of all six spheres (inner diameters of 37, 28, 22, 17, 13, and 10 mm) in the phantom were measured using a VOI that covered the entire sphere, and recorded for all reconstructed images.

Table 1. Time calculations for image reconstruction.

Reconstruction No.	Time (min:sec)	Duration (min:sec)	Decay factor
1	(A)	2:00	1
2	(A) + 2:00	2:02	0.987
3	(A) + 4:02	2:03	0.975
4	(A) + 6:05	2:05	0.962
5	(A) + 8:10	2:06	0.950
6	(A) + 10:16	2:08	0.937

At the time (A), the total radioactivity in the phantom corresponds to 2.53 kBq/cc

Decay factor = $e^{-\frac{\text{elapsed time after(A)}}{\text{half life}}\times\ln(2)}$

Duration = 2 min / Decay factor, e.g., Duration for reconstruction no. 2 = 2 min / 0.987

https://doi.org/10.1371/journal.pone.0192549.t001

Recovery coefficient

The recovery coefficient (RC) for a *j*-mm-diameter hot sphere (RC_j) is the quotient of the maximum pixel value (C_j) within the region of interest over the sphere on the reconstructed image and the maximum pixel value of a 37-mm-diameter sphere (C_{37}): $RC_j = {}^{C_j}/_{C_{37}}$. These coefficients are calculated using the averaged values obtained from all 50 images. Additionally, the values obtained from the image corresponding to the 30-min acquisition were also calculated as the standard RCs.

Repeatability

To evaluate the repeatability of the SUVs measured by the two scanners, Bland-Altman plot analyses were performed.

Results

The total radioactivity of the ^{18}F-FDG solution at the time of phantom preparation was 37.9 MBq (3.84 kBq/cc) for the *Celesteion* scanner, and 27.3 MBq (2.77 kBq/cc) for the *Aquiduo*. As mentioned in the Methods section, we set the start of image reconstruction at the time when the total radioactivity in the phantom was 2.53 kBq/cc, and used the counts for the first 2-min acquisition period as the standard. Before we demonstrate the results of our count-based reconstruction method, we show the trend of measured SUVs obtained with a constant acquisition period in Fig 1. The SUV_{max} and SUV_{peak} of the 37-mm-diameter sphere are shown for constant 2-min acquisition periods using the *Celesteion* scanner. The x-axis represents the time after scanning commenced. The SUVs tended to increase, especially the SUV_{max}. The SUV_{max} also exhibited a gradual increase in variation over time. Results obtained using the *Aquiduo* are omitted.

Variations of measured SUVs

Fig 2 shows the distributions of the SUV_{max} and SUV_{peak}, respectively, of three of the six spheres (inner diameter of Sphere; 37 mm, 22 mm and 13 mm). The increasing tendencies of the values and variations were not obvious for both SUV_{max} and SUV_{peak}.

Table 2 summarises the mean and standard deviation (SD) values of the measured SUVs.

Repeatability of SUVs

Fig 3 depicts the Bland-Altman plots of the SUVs for three of the six spheres measured by the *Celesteion* and *Aquiduo* scanners.

The mean, SD, and 95% confidence interval (CI) values are shown in Table 3.

Recovery coefficient

The curves of the recovery coefficients measured by the *Celesteion* and *Aquiduo* scanners are depicted in Fig 4. The *Celesteion* scanner demonstrated higher recovery coefficients than the *Aquiduo* scanner, particularly at a diameter of approximately 20 mm. Additionally, the curves calculated from the averaged values of the count-based images exhibited lower values than those calculated from the 30-min acquisition images.

Discussion

It is important to develop an easy and robust method to evaluate the variability and repeatability of measured SUVs, not only for daily PET examinations, but also for multi-institutional studies. Repetitive phantom scans provide valuable information regarding the characteristics

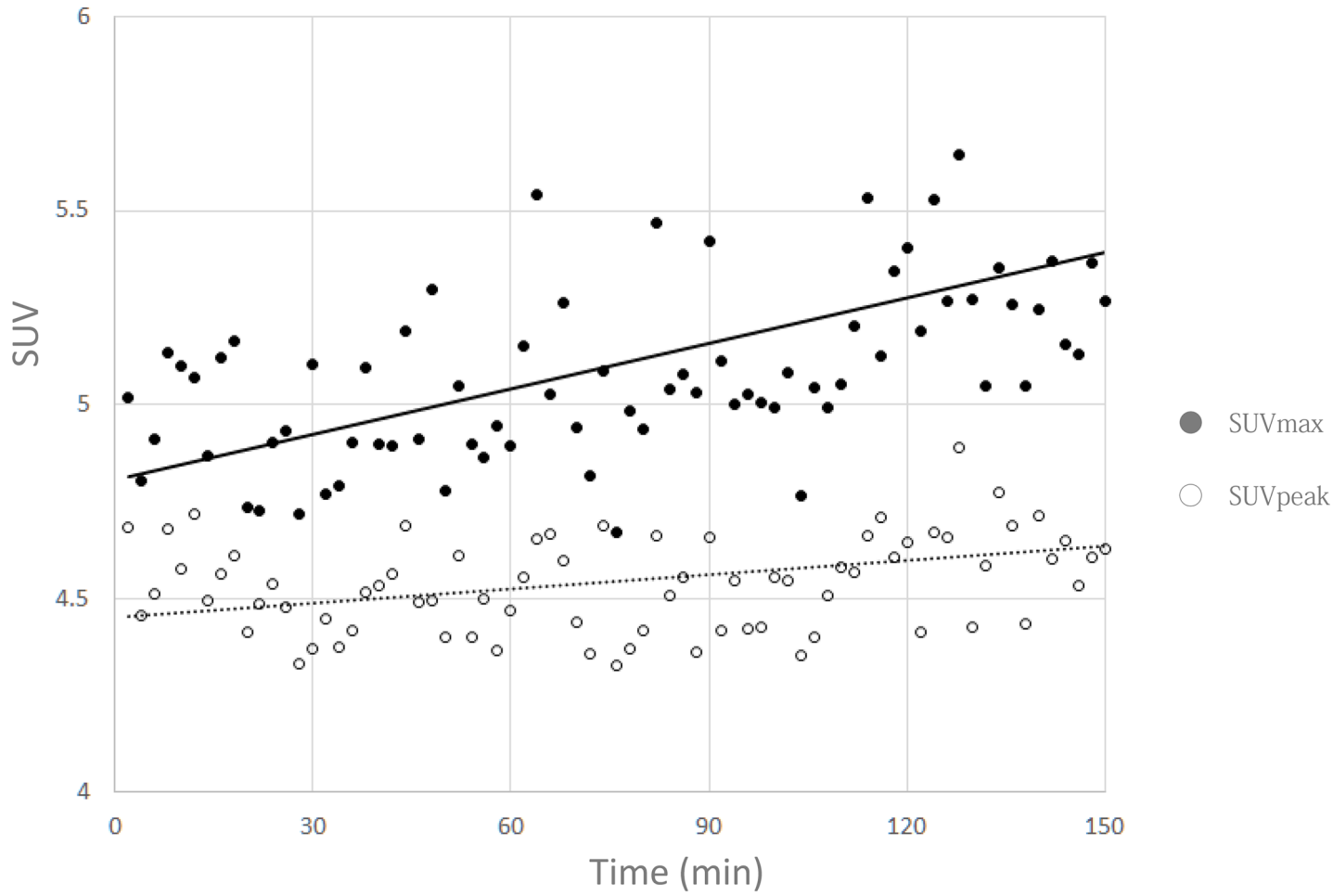

Fig 1. The measured SUV_{max} and SUV_{peak} of a 37-mm-diameter sphere with a 2-min acquisition over time. Standardized uptake values (SUVs) obtained from constant 2-min acquisition periods using the *Celesteion* scanner are shown over time to compare the resulting SUVs. The scatter plot depicts SUV_{max} (solid, black circle) and SUV_{peak} (empty/open circle) values. The solid and dotted trend lines correspond to SUV_{max} and SUV_{peak}, respectively.

https://doi.org/10.1371/journal.pone.0192549.g001

of the scanner and workstation. However, as demonstrated in Fig 1, simple repetitive scans with fixed acquisition times demonstrate the tendency of the measured SUVs to increase, mainly due to the increase of noise from the decay of radioactivity [10]. To avoid the influence of radioactivity changes, the total counts for each image reconstruction should be fixed. However, the list-mode data contains information regarding the time of the counts, but not the order of the counts. Thus, it is difficult to set a fixed count threshold for each image. Thus, we developed a method to calculate the reconstruction time to maintain the counts for each image. In this study, we applied the radioactivity and acquisition times of common clinical FDG-PET studies: 2.53 kBq/cc of radioactivity at the beginning of the PET scan, and a 2-min scan for a bed position. We also operated the PET scanners under the same conditions as those of daily clinical PET examinations. To our knowledge, this is the first study that has propounded count-based image reconstruction for the evaluation of variation and repeatability of measured SUVs. We believe that our method could apply to the standardization and harmonization of SUVs in multi-institutional studies.

Our results clearly demonstrated the differences between the SUVs measured by the two different scanners. The SUVs measured by the older scanner (*Aquiduo*) were 10–30% smaller

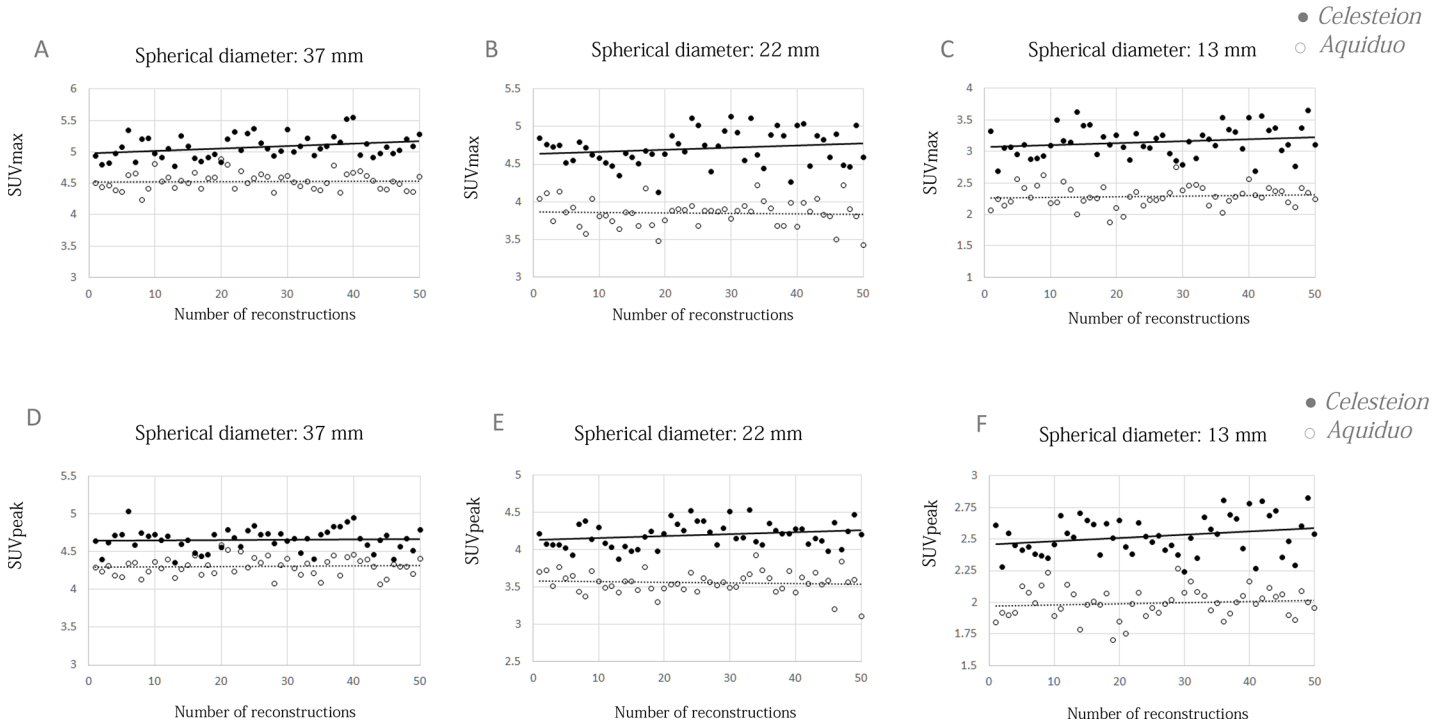

Fig 2. The distributions of count-based measured SUV_{max} and SUV_{peak}. The distribution of the SUV_{max} (A-C) and SUV_{peak} (D-F) of the representative three spheres. The 50 count-based measurements were performed using the *Celesteion* (solid, black circle) and *Aquiduo* (empty/open circle) scanners. The solid and dotted trend lines correspond to the *Celesteion* and *Aquiduo*, respectively.

https://doi.org/10.1371/journal.pone.0192549.g002

than those measured by the newer scanner (*Celesteion*). In our hospital, these scanners have been used with equal frequency. A considerable number of patients have been examined with each scanner. Such differences in SUVs may cause misinterpretation of the PET examination results. When more than one scanner is used, harmonization or calibration of SUVs is required.

Our results also suggested that the SD of the measured SUVs was between 0.1 and 0.2. There was a tendency for the smaller sphere to exhibit a larger SD, and the SUV_{peak} had a smaller SD than the SUV_{max}. These results can be explained by the noise effect. The small

Table 2. Mean and standard deviation (SD) of measured SUVs.

Diameter of the sphere	37mm	22mm	13mm
Celesteion			
SUV_{max} Mean	5.077	4.707	3.150
SD	0.146	0.189	0.194
SUV_{peak} Mean	4.657	4.194	2.523
SD	0.112	0.136	0.125
Aquiduo			
SUV_{max} Mean	4.534 (89.3%)	3.848 (81.8%)	2.291 (72.7%)
SD	0.110	0.135	0.132
SUV_{peak} Mean	4.303 (92.3%)	3.560 (84.9%)	1.994 (79.0%)
SD	0.095	0.109	0.090

The percentage in parentheses represents the ratio to the SUVs measured by *Celesteion*.

https://doi.org/10.1371/journal.pone.0192549.t002

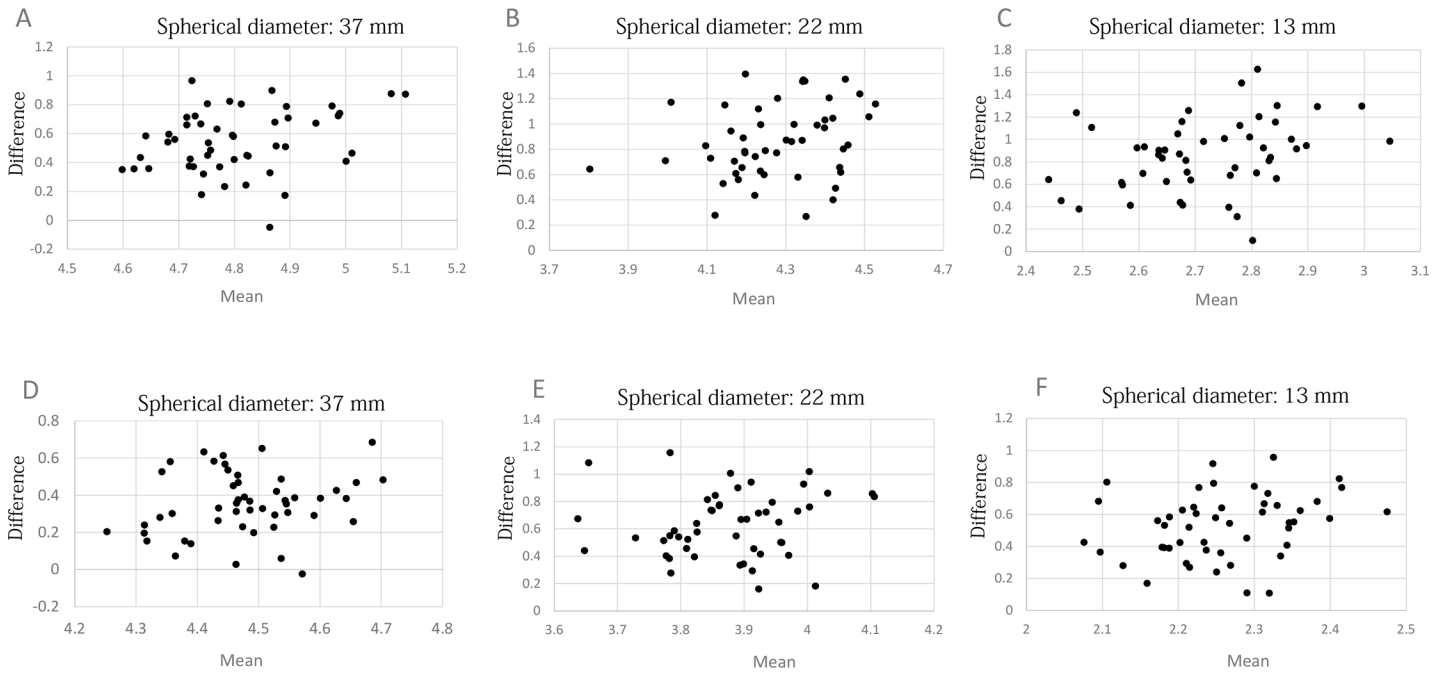

Fig 3. The Bland-Altman plots of count-based measured SUV_{max} and SUV_{peak}. The Bland-Altman plots of SUV_{max} (A-C) and SUV_{peak} (D-F) measured by the *Celesteion* and *Aquiduo*.

https://doi.org/10.1371/journal.pone.0192549.g003

amount of radioactivity that occurs due to the small size of the sphere increases the noise. The SUV_{max} is influenced more by the noise than the SUV_{peak}, because the SUV_{max} represents the highest value in the VOI. A SD between 0.1 and 0.2 seems to be tolerable for the evaluation of clinical PET examinations, because it has been reported that tumor SUV has a within-subject coefficient of variation of approximately 10% [14]. The guidelines of clinical PET examinations and PET scanner maintenance could include the use of the SD measured with our method as an assessment criterion.

The results of the Bland-Altman analyses demonstrated poor agreement between the SUVs measured by the two scanners. The SD of the difference was several times larger than the 95% CI. We do not think that such a poor agreement was a result of unsatisfactory phantom preparation, but rather a result of the short acquisition times, corresponding to 2 min. The images obtained from such short samples have considerable noise, but comparable acquisition periods

Table 3. The results of Bland-Altman analyses of the SUVs measured by the *Celesteion* and *Aquiduo* scanners.

Diameter of the sphere (mm)	37	28	22	17	13	10
SUV_{max}						
Difference Mean	0.543	0.587	0.859	0.969	0.859	0.590
SD	0.177	0.196	0.237	0.253	0.251	0.215
95% CI	0.049	0.054	0.066	0.070	0.070	0.060
SUV_{peak}						
Difference Mean	0.354	0.391	0.634	0.734	0.530	0.315
SD	0.132	0.167	0.194	0.164	0.163	0.130
95% CI	0.037	0.046	0.054	0.045	0.045	0.036

SD = standard deviation, CI = confidence interval

https://doi.org/10.1371/journal.pone.0192549.t003

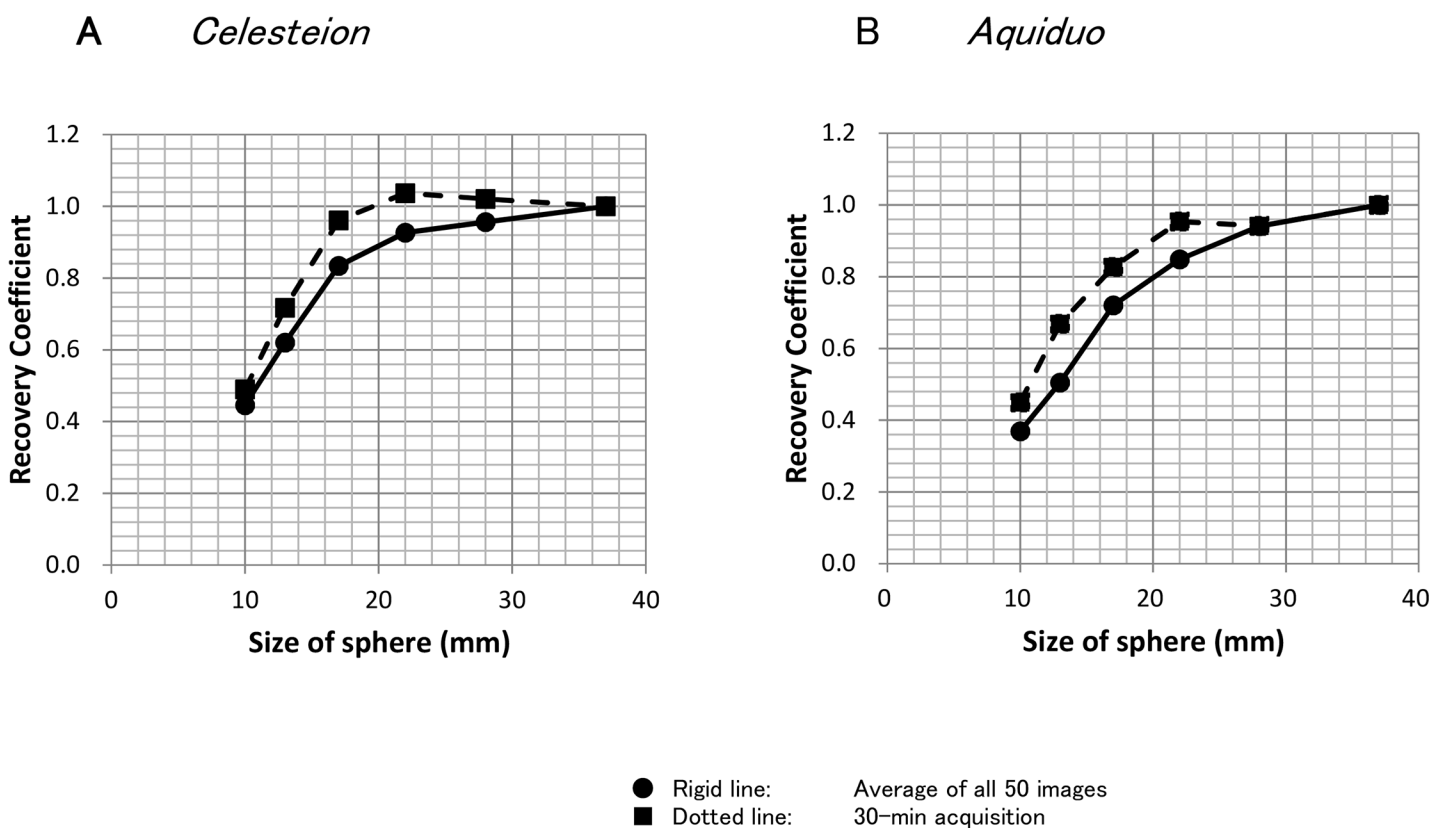

Fig 4. The curves of the recovery coefficients. The curves of the recovery coefficients measured by the *Celesteion* (a) and *Aquiduo* (b) scanners. The solid line with black circles corresponds to the average of the count-based measurements. The dashed line with black squares corresponds to the standard 30-min acquisition measurements.

https://doi.org/10.1371/journal.pone.0192549.g004

are commonly used in clinical settings. The large SD of the measured SUVs may suggest fragility of SUVs as an imaging biomarker, and should be taken into account when we interpret SUVs of a lesion.

As our results demonstrated, there were considerable differences in the recovery coefficients between the two scanners. This may be due to the newer scanner's (*Celesteion*) better special resolution. Such technological improvements often lead to significant device-dependent and reconstruction-dependent variations in quantitative values. The European Association of Nuclear Medicine Research Ltd. (EARL) accreditation program [15], the North American QIBA, and the Uniform Protocols in Clinical Trials (UPICT) [16] all recommend that adequate reproducibility of SUVs be achieved by patient preparation, as well as acquisition and reconstruction parameters. It was recently shown that it is possible to harmonize SUVs by applying the Gaussian filters [17]. This method requires the recovery coefficients calculated from the images of a NEMA IEC body phantom. However, such phantom images have been generally obtained with much longer (10–30 min) acquisition times than that of a daily oncology PET examination (approximately 2 min/bed). As shown in Fig 4, the differences in the acquisition times result in differences in the recovery coefficients. From this perspective, we suggest the use of the averaged values obtained from count-based image reconstruction, under the same conditions as actual clinical settings. Using such values obtained from another scanner, we can harmonize SUVs between the two scanners. For example, our results showed that an SUV of 4.0 for a 22-mm-diameter sphere was measured as an SUV_{max} of 4.7 by the

Celesteion and of 3.8 by the Aquiduo. We can harmonize the SUV_{max} of 4.7 obtained by the Celesteion with the value of 3.8 obtained by the Aquiduo, or the other way around. Alternatively, SUV_{max} values from both the Celesteion and Aquiduo could be calibrated to the actual SUV of 4.0, which can be called as a standardization. The measured SUVs depend mainly on the size of lesion and the actual SUV [10]. Thus, it is necessary to evaluate a phantom that is set for several SUVs. Correction for partial volume effects might also be useful for small lesions [18]. Validation of these methods using clinical data is required, and this will be a subject for further study.

There is a limitation of our count-base method. Some of the trend lines of SUVs in Fig 2 show a slight upward trend. This may suggest that our method is limited in its ability to correct the counts in each reconstruction. Our method cannot exclude the influence of random coincidences, statistical noise, or dead-time losses. The noise equivalent count rate of the scanner may be useful for further correction.

Conclusions

We propose the use of count-based image reconstruction to obtain a considerable number of images under clinical settings from hours of list-mode scanning. These results are useful for evaluating the variability and repeatability of measured SUVs. The results for various scanners are also useful for standardization and harmonization of SUVs in multi-institutional studies.

Acknowledgments

No human subjects or animals were enrolled in this study. Thus, neither institutional review board approval nor informed consent were applicable to this study.

Author Contributions

Conceptualization: Tomohiro Kaneta, Hiromitsu Daisaki.

Data curation: Tomohiro Kaneta, Matsuyoshi Ogawa, En-Tao Liu, Hitoshi Iizuka, Tetsu Arisawa.

Formal analysis: Tomohiro Kaneta, Matsuyoshi Ogawa, En-Tao Liu, Ayako Hino-Shishikura.

Investigation: Keisuke Yoshida.

Methodology: Tomohiro Kaneta, Hiromitsu Daisaki.

Software: Hiromitsu Daisaki.

Supervision: Tomio Inoue.

Writing – original draft: Tomohiro Kaneta.

Writing – review & editing: Hitoshi Iizuka, Keisuke Yoshida, Tomio Inoue.

References

1. Dehdashti F, Siegel BA, Griffeth LK, Fusselman MJ, Trask DD, McGuire AH, et al. Benign versus malignant intraosseous lesions: discrimination by means of PET with 2-[F-18]fluoro-2-deoxy-D-glucose. Radiology. 1996; 200:243–247. https://doi.org/10.1148/radiology.200.1.8657920 PMID: 8657920
2. Song BI, Lee SW, Jeong SY, Chae YS, Lee WK, Ahn BC, et al. 18F-FDG uptake by metastatic axillary lymph nodes on pretreatment PET/CT as a prognostic factor for recurrence in patients with invasive ductal breast cancer. J Nucl Med. 2012; 53:1337–1344. https://doi.org/10.2967/jnumed.111.098640 PMID: 22870824
3. Song BI, Kim HW, Won KS, Ryu SW, Sohn SS, Kang YN. Preoperative Standardized Uptake Value of Metastatic Lymph Nodes Measured by 18F-FDG PET/CT Improves the Prediction of Prognosis in

Gastric Cancer. Medicine (Baltimore). 2015; 94(26):e1037. https://doi.org/10.1097/MD.0000000000001037 PMID: 26131811

4. Kitajima K, Suenaga Y, Kanda T, Miyawaki D, Yoshida K, Ejima Y, et al. Prognostic value of FDG PET imaging in patients with laryngeal cancer. PLoS One. 2014; 9(5):e96999. https://doi.org/10.1371/journal.pone.0096999 PMID: 24818750
5. Berghmans T, Dusart M, Paesmans M, Hossein-Foucher C, Buvat I, Castaigne C, et al. Primary tumor standardized uptake value (SUV_{max}) measured on fluorodeoxyglucose positron emission tomography (FDG-PET) is of prognostic value for survival in non-small cell lung cancer (NSCLC): a systematic review and meta-analysis (MA) by the European Lung Cancer Working Party for the IASLC Lung Cancer Staging Project. J Thorac Oncol. 2008; 3(1):6–12. https://doi.org/10.1097/JTO.0b013e31815e6d6b PMID: 18166834
6. Beaulieu S, Kinahan P, Tseng J, Dunnwald LK, Schubert EK, Pham P, et al. SUV varies with time after injection in (18)F-FDG PET of breast cancer: characterization and method to adjust for time differences. J Nucl Med. 2003; 44:1044–1050. PMID: 12843218
7. Keyes JW Jr. SUV: standard uptake or silly useless value? J Nucl Med. 1995; 36:1836–39. PMID: 7562051
8. Lodge MA, Chaudhry MA, Wahl RL. Noise considerations for PET quantification using maximum and peak standardized uptake value. J Nucl Med. 2012; 53:1041–1047. https://doi.org/10.2967/jnumed.111.101733 PMID: 22627001
9. Sullivan DC, Obuchowski NA, Kessler LG, Raunig DL, Gatsonis C, Huang EP, et al. Metrology Standards for Quantitative Imaging Biomarkers. Radiology. 2015; 277:813–825. https://doi.org/10.1148/radiol.2015142202 PMID: 26267831
10. Kaneta T, Sun N, Ogawa M, Iizuka H, Arisawa T, Hino-Shishikura A, et al. Variation and repeatability of measured standardized uptake values depending on actual values: a phantom study. Am J Nucl Med Mol Imaging. 2017 Nov 1; 7(5):204–211. PMID: 29181267
11. National Electrical Manufacturers Association. Performance measurements of positron emission tomographs. NEMA Standards Publication NU 2–2012. Rosslyn, USA: National Electical Manufacturers Association. 2012.
12. Nagaki A, Onoguchi M, Matsutomo N. CT tube current for attenuation map in a combined PET/CT system: obese patient simulated phantom study. Ann Nucl Med. 2012; 26(4):359–64. https://doi.org/10.1007/s12149-012-0584-5 PMID: 22359224
13. Kaneta T, Ogawa M, Motomura N, Iizuka H, Arisawa T, Hino-Shishikura A, et al. Initial evaluation of the Celesteion large-bore PET/CT scanner in accordance with the NEMA NU2-2012 standard and the Japanese guideline for oncology FDG PET/CT data acquisition protocol version 2.0. EJNMMI Res. 2017 Oct 11; 7(1):83. https://doi.org/10.1186/s13550-017-0331-y PMID: 29022216
14. Lodge MA. Repeatability of SUV in Oncologic ^{18}F-FDG PET. J Nucl Med. 2017 Apr; 58(4):523–532. https://doi.org/10.2967/jnumed.116.186353 PMID: 28232605
15. Boellaard R, Delgado-Bolton R, Oyen WJ, Giammarile F, Tatsch K, Eschner W, et al. FDG PET/CT: EANM procedure guidelines for tumour imaging: version 2.0. Eur J Nucl Med Mol Imaging. 2015; 42:328–54. https://doi.org/10.1007/s00259-014-2961-x PMID: 25452219
16. Graham MM, Wahl RL, Hoffman JM, Yap JT, Sunderland JJ, Boellaard R, et al. Summary of the UPICT protocol for ^{18}F-FDG PET/CT imaging in oncology clinical trials. J Nucl Med. 2015; 56:955–61. https://doi.org/10.2967/jnumed.115.158402 PMID: 25883122
17. Lasnon C, Desmonts C, Quak E, Gervais R, Do P, Dubos-Arvis C, et al. Harmonizing SUVs in multicentre trials when using different generation PET systems: prospective validation in non-small cell lung cancer patients. Eur J Nucl Med Mol Imaging. 2013; 40:985–96. https://doi.org/10.1007/s00259-013-2391-1 PMID: 23564036
18. Boussion N, Cheze Le Rest C, Hatt M, Visvikis D. Incorporation of wavelet-based denoising in iterative deconvolution for partial volume correction in whole-body PET imaging. Eur J Nucl Med Mol Imaging. 2009 Jul; 36(7):1064–75. https://doi.org/10.1007/s00259-009-1065-5 PMID: 19224209